Journal of Materials Chemistry A

Self-assembly synthesis and electrochemical performance of the Li1.5Mn0.75Ni0.15Co0.10O2+δ microspheres with multilayer shells

Journal:	*Journal of Materials Chemistry A*
Manuscript ID:	TA-ART-10-2014-005281.R2
Article Type:	Paper
Date Submitted by the Author:	30-Nov-2014
Complete List of Authors:	yu, ruizhi; Xiangtan University, shool of chemistry wang, xianyou; Xiangtan University, shool of chemistry wang, di; Xiangtan University, school of chemistry ge, long; Xiangtan University, school of chemistry shu, hongbo; Xiangtan University, school of chemistry yang, xiukang; Xiangtan University, school of chemistry

Self-assembly synthesis and electrochemical performance of the $Li_{1.5}Mn_{0.75}Ni_{0.15}Co_{0.10}O_{2+\delta}$ microspheres with multilayer shells

Ruizhi Yu, Xianyou Wang*, Di Wang, Long Ge, Hongbo Shu, Xiukang Yang*

(Key Laboratory of Environmentally Friendly Chemistry and Applications of Ministry of Education, Hunan Province Key Laboratory of Electrochemical Energy Storage and Conversion, School of Chemistry, Xiangtan University, Hunan, Xiangtan 411105, China)

Abstract

The novel $Li_{1.5}Mn_{0.75}Ni_{0.15}Co_{0.10}O_{2+\delta}$ microspheres with hierarchically multilayer shells are rationally designed and successfully prepared through layer-by-layer self-assembly deposit with a co-precipitation process. The microsphere with multilayer shells is consisted of $Li_{1.5}Mn_{0.75}Ni_{0.25}O_{2+\delta}$ inner core and hierarchically multilayer shells. The structure and electrochemical properties of the spherical $Li_{1.5}Mn_{0.75}Ni_{0.15}Co_{0.10}O_{2+\delta}$ cathode material with multilayer shells are evaluated and compared to those of the conventional $Li_{1.5}Mn_{0.75}Ni_{0.15}Co_{0.10}O_{2+\delta}$ cathode material with the same chemical composition as the multilayer spherical cathode material. The results show that the spherical cathode material with multilayer shells delivers a high discharge capacity of 257.8 mAh g^{-1} at a rate of 0.1 C with outstanding capacity retention of 96.1% after 100 cycles at 0.5 C between 2.0 and 4.6 V. Especially, the spherical cathode material with multilayer shells exhibits an improved rate capability with capacity of 102.7 mAh g^{-1} even at a high discharge rate of 10 C, it is apparently

* **Corresponding author:** Xianyou Wang, Xiukang Yang, Tel: +86 731 58292060; Fax: +86 731 58292061.
E-mail address: wxianyou@yahoo.com (X. Wang), yshowk23@163.com (X. Yang)

superior to the conventional $Li_{1.5}Mn_{0.75}Ni_{0.15}Co_{0.10}O_{2+\delta}$ cathode material (64.9 mAh g^{-1}). Thus, reasonable design for function and structure of cathode material will be a significant work for improving lithium ion battery performance.

Keywords: Lithium-ion batteries; Lithium-rich layered cathode material; Hierarchically multilayer shells; Co-precipitation method

1. Introduction

As the influence of global warming and energy crisis increases severely, the development of sustainable energy becomes the emphasis of current research. Lithium-ion batteries are considered to be a good option for the solution of the problems and paid more and more attention in recent years, due to the features of high power densities and environmental benefits.[1-3] Nowadays, lithium-ion batteries have been widely used in portable electronics, such as laptops, tablet computers, cellphones and so on. In addition, lithium-ion batteries are the most promising power sources of electric vehicles (EVs) and hybrid electric vehicles (HEVs) that most probably become the next generation of green transportation.[4] The rise of commercialized EVs and HEVs could depend in large part on whether researchers can enhance energy density and reduce costs of lithium-ion batteries. It's a common knowledge that the energy density and costs are mainly limited by the cathode materials. Thus, the key of power lithium-ion batteries is the successful exploitation of cathode materials with high performance and low costs.[3]

Recently, lithium-rich layered cathode material, $Li_{1+x}[M]_{1-x}O_2$ (M = Mn, Ni, Co, etc.

$0 < x < 1$) has been the hot spot in the research of cathode materials due to its remarkably high discharge capacity of over 250 mAh g^{-1} when cycled in the voltage of over 4.5 V.[5-9] This kind of material can also be represented using structurally integrated two-component solid solution notations $x$$Li_2MnO_3$·(1-$x$)$LiMO_2$ (M = Mn, Ni, Co, etc. $0 < x < 1$).[5] The component of Li_2MnO_3 plays the important role to enhance the properties of $x$$Li_2MnO_3$·(1-$x$)$LiMO_2$, during charge/discharge process. Some studies have shown that the long plateau region that began at ~4.5 V corresponds to the extraction of Li^+ from the lattice of Li_2MnO_3 component accompanying the oxygen loss, in the initial charge.[10, 11] The irreversible removal of Li^+ accompanied by oxygen evolution can facilitate the lowering of the oxidation states of the transition metal ions, and thus can result in high reversible capacities in following charge/discharge cycles.[12] In addition, the inexpensive Mn element serves as a substitute for costly Ni and Co elements, which can reduce the production costs.

Although the lithium-rich layered cathode material has so many advantages, there are still several unsolved issues hindering the large-scale commercial popularization of the material, such as low coulombic efficiency, poor rate capability, and significant decrease in capacity with successive cycling. To resolve these problems, a collection of solutions have been proposed. For example, element doping is an efficient strategy to enhance the structural stability of the lithium-rich layered cathode material. But it can cause a fading of capacity because the substituents are usually electrochemically inactive elements.[13-15] Recently, a method of fabricating cathode materials with core-shell structure is proposed as a new idea of materials design.[16-19] Generally

speaking, the core can deliver high capacity, whereas the shell provides high structural stability.[16] This approach can improve the deficiencies of the element doping method, and enhance significantly the performance of the cathode materials. In addition, some new materials with hollow micro/nanostructure and double-shelled hollow structure also have caused a great concern.[20, 21] These extraordinary structures are often associated with fast Li^+ diffusion, leading to better rate capability. Moreover, the interior void space can buffer the periodical volume change of the electrode materials during Li^+ insertion/extraction process.[20, 22]

Based on above points, herein, we reasonably designed and synthesized a kind of innovative spherical $Li_{1.5}Mn_{0.75}Ni_{0.15}Co_{0.10}O_{2+\delta}$ microspheres with hierarchically multilayer shells structure via layer-by-layer self-assembly with a co-precipitation process. The microsphere with multilayer shells is made up of an inner core $Li_{1.5}Mn_{0.75}Ni_{0.25}O_{2+\delta}$ and hierarchically multilayer shells. The spherical cathode material with multilayer shells is the perfect combination of advantages of both core-shell structure and hollow structure materials. The structures, morphologies and electrochemical properties of the spherical $Li_{1.5}Mn_{0.75}Ni_{0.15}Co_{0.10}O_{2+\delta}$ cathode material with multilayer shells were studied in detail.

2. Experimental

2.1 Synthesis of the spherical cathode material with multilayer shells and conventional cathode material

According to our strategy for novel cathode material, the precursor should have an

inner core and a multi-component shell with increasing Co content and decreasing Ni content step by step towards to the outer surface of the particle, while the Mn concentration remains constant throughout the particle. To prepare the spherical $Li_{1.5}[Mn_{0.75}Ni_{0.15}Co_{0.10}]O_{2+\delta}$ cathode material with multilayer shells, the precursor was synthesized firstly by co-precipitation method as our previous report.[23] Scheme 1 shows an illustration of the co-precipitation process. During this reaction process, two kinds of solution with different metal ions were needed. One was a mixed aqueous solution of $NiSO_4$ and $MnSO_4$ (Ni:Mn = 1:3, molar ratio) with a concentration of 1.6 mol L^{-1} which was named solution A, another was a mixed aqueous solution of $CoSO_4$ and $MnSO_4$ (Co:Mn = 1:3, molar ratio, 1.6 mol L^{-1}) which was named solution B. The solution A and solution B were separately placed in tank 1 and tank 2. At the beginning of the reaction, the solution A was firstly pumped into a stirred tank reactor in designed flow rate. At the same time, a 1.6 mol L^{-1} Na_2CO_3 solution as precipitant and desired amount of $NH_3 \cdot H_2O$, solution as chelating agent were separately fed into the reactor. After one hour, the spherical $[Mn_{0.75}Ni_{0.25}]CO_3$ core precursor particles were formed. Then, the solution B placed in tank 2 was intermittently pumped into tank 1 (the volume of solution A was 1.5 times of B). Simultaneously, the mixed solution of A and B was stirred and fed into the stirred reactor. The hierarchically multilayer shells with increasing Co content and decreasing Ni content were deposited through layer-by-layer self-assembly onto the surface of the core precursor particles. The pH, temperature, and stirring speed of the mixture in the reactor were set to 7.5, 55 °C, and 600 rpm, these conditions must be controlled strictly to ensure that the

reaction products were uniform spherical particles. As the reaction proceeded, the $[Mn_{0.75}Ni_{0.25}]CO_3$ core was encapsulated completely within a stable multi-component shell. The obtained precursor was aged for 12 h, then filtered, washed and dried overnight at 110 °C. Thenceforth, the precursor was pre-sintered at 500 °C for 6 h for converting into oxide powder. Finally, the oxide powder was mixed with appropriate amount of Li_2CO_3, calcined at 850 °C for 12 h, and cooled to room temperature.

For comparison, the conventional $Li_{1.5}[Mn_{0.75}Ni_{0.15}Co_{0.10}]O_{2+\delta}$ cathode material was also synthesized via the co-precipitation process. The mixed solution of $NiSO_4$, $CoSO_4$ and $MnSO_4$ (Ni:Co:Mn = 3:2:15 in molar ratio, 1.6 mol L^{-1}) was continuously pumped into a stirred tank in designed flow rate to prepare the conventional $[Mn_{0.75}Ni_{0.15}Co_{0.10}]CO_3$ precursor. At the same time, Na_2CO_3 solution and $NH_3{\cdot}H_2O$ solution were separately fed into the reactor. The following preparation process of the conventional $Li_{1.5}[Mn_{0.75}Ni_{0.15}Co_{0.10}]O_{2+\delta}$ cathode material was the same as the spherical $Li_{1.5}[Mn_{0.75}Ni_{0.15}Co_{0.10}]O_{2+\delta}$ cathode material with multilayer shells.

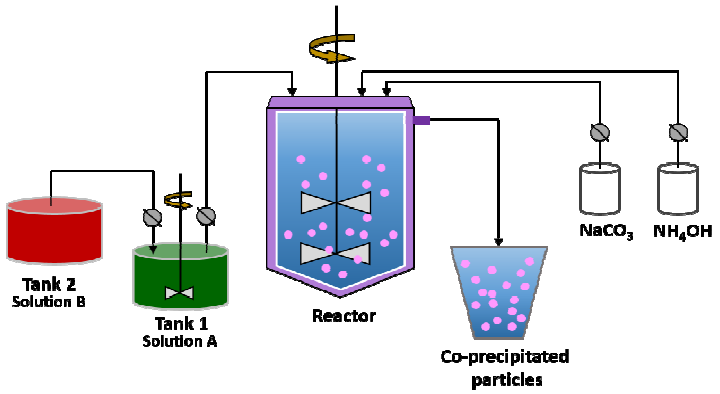

Scheme 1 Schematic illustration of co-precipitation process; Tank 1: Mixed solution of $NiSO_4$ and $MnSO_4$ (Ni:Mn = 1:3, molar ratio), Tank 2: Mixed solution of $CoSO_4$ and $MnSO_4$ (Co:Mn = 1:3, molar ratio).

2.2 Materials characterization

In order to determine the chemical composition of the as-prepared materials, atomic absorption spectroscopy (AAS, Vario 6 Analytik Jena AG, Jena) analysis was carried out. The morphology and atomic concentration of the samples were examined with a scanning electron microscopy (SEM) equipped with an energy-dispersive X-ray spectroscope (EDXS) (JSM-6100LV, JEOL, Japan). A X-ray diffractometer (D/Max-3C, Rigaku, Japan) using Cu Kα radiation (λ = 0.154178 nm) and a graphite monochromator at 36 kV, 20 mA was employed to identify the crystalline phase of the resulting cathode materials, the scanning rate was 4 °min^{-1} and the scanning range of diffraction angle (2θ) was between 10° and 80°.

2.3 Electrochemical test

The positive electrodes were fabricated by coating a paste of 80 wt % active substances of the prepared cathode materials, 5 wt % acetylene black, 5 wt % graphite and 10 wt % polyvinylidene fluoride (PVDF) binder onto aluminum foils, with N-methylpyrrolidone (NMP) as the solvent. The coated foils were then roll-pressed and dried at 80 °C for 12 h in an oven. Finally, the positive films were cut into circular electrodes of 10 mm diameter and dried overnight at 110 °C in a vacuum oven before use. Generally, the mass of the positive active material is about 4 mg per electrode. The electrochemical tests were performed with CR2025 coin cells assembled in a glove box under argon atmosphere using a Lithium metal foil as the anode. The electrolyte solution was 1 mol L^{-1} $LiPF_6$ in ethylene carbonate (EC)-dimethyl carbonate (DMC) (1:1, V:V). Moreover, a porous polypropylene based membrane

(Celgard) was used as the separator. The charge/discharge characteristics of the final cathode materials were determined by potential cycling at different current densities in the voltage range of 2.0-4.6 V (vs Li^+/Li). Especially, the cells were firstly charged at 0.2 C and discharged at various rates to evaluate the rate performance of the materials. These tests were based on a constant current method. Galvanostatic intermittent titration technique (GITT) was collected by charging/discharging a cell for a given time period (10 min) at a constant current flux of 0.05 C, then keeping the cell in an open-circuit (OCV) voltage for 60 min. The procedure was completed until the full voltage range (2.0-4.6 V) was covered. All the tests were run at 25 °C.

3. Results and discussion

The total average chemical composition of the as-prepared samples was determined by AAS. Table 1 shows the designed and measured chemical compositions of the obtained precursors and final lithiated cathode materials. It can be seen that all of the measured chemical compositions of the as-prepared samples are well matched with the designed values. The spherical cathode material with multilayer shells was founded to be $Li_{1.51}[Mn_{0.749}Ni_{0.147}Co_{0.104}]O_{2+\delta}$, and it's close to the desired chemical formula.

Table 1 Designed and measured chemical compositions of the obtained samples

	Designed composition	Measured composition
Conventional precursor	$[Mn_{0.75}Ni_{0.15}Co_{0.10}]CO_3$	$[Mn_{0.752}Ni_{0.145}Co_{0.103}]CO_3$
Conventional cathode material	$Li_{1.5}[Mn_{0.75}Ni_{0.15}Co_{0.10}]O_{2+\delta}$	$Li_{1.50}[Mn_{0.750}Ni_{0.146}Co_{0.104}]O_{2+\delta}$
Multilayer precursor	$[Mn_{0.75}Ni_{0.15}Co_{0.10}]CO_3$	$[Mn_{0.753}Ni_{0.142}Co_{0.105}]CO_3$

Multilayer cathode material	$Li_{1.5}[Mn_{0.75}Ni_{0.15}Co_{0.10}]O_{2+\delta}$	$Li_{1.51}[Mn_{0.749}Ni_{0.147}Co_{0.104}]O_{2+\delta}$

The morphologies of the precursors were performed using SEM, as well as their corresponding lithiated cathode materials. Fig. 1a and b display the SEM images of multilayer $[Mn_{0.75}Ni_{0.15}Co_{0.10}]CO_3$ (denoted by MP) and conventional $[Mn_{0.75}Ni_{0.15}Co_{0.10}]CO_3$ (denoted by CP) precursors, respectively. Both of the MP and CP precursors show analogous morphology with a spherical shape and 8 μm in diameter approximately, which are formed with agglomerates of nano-sized primary grains. These features of the precursor particles are similar to previous reports of carbonate particles prepared via co-precipitation.[24, 25] Fig. 1c and d display the SEM images of the spherical $Li_{1.5}[Mn_{0.75}Ni_{0.15}Co_{0.10}]O_{2+\delta}$ with multilayer shells (denoted by MSL) and conventional $Li_{1.5}[Mn_{0.75}Ni_{0.15}Co_{0.10}]O_{2+\delta}$ (denoted by CL) cathode materials, respectively. It can be seen that both the MSL and CL cathode materials are maintained the spherical morphology, after lithiation at high temperature. However, the primary grains of the lithiated cathode materials tend to grow up compared to the precursors. In addition, some small holes can be observed in the surfaces of the MSL and CL cathode materials, which are probably caused by the emission of CO_2 gas during the calcination process. Furthermore, there are no obvious differences can be observed between the SEM images of these two cathode materials.

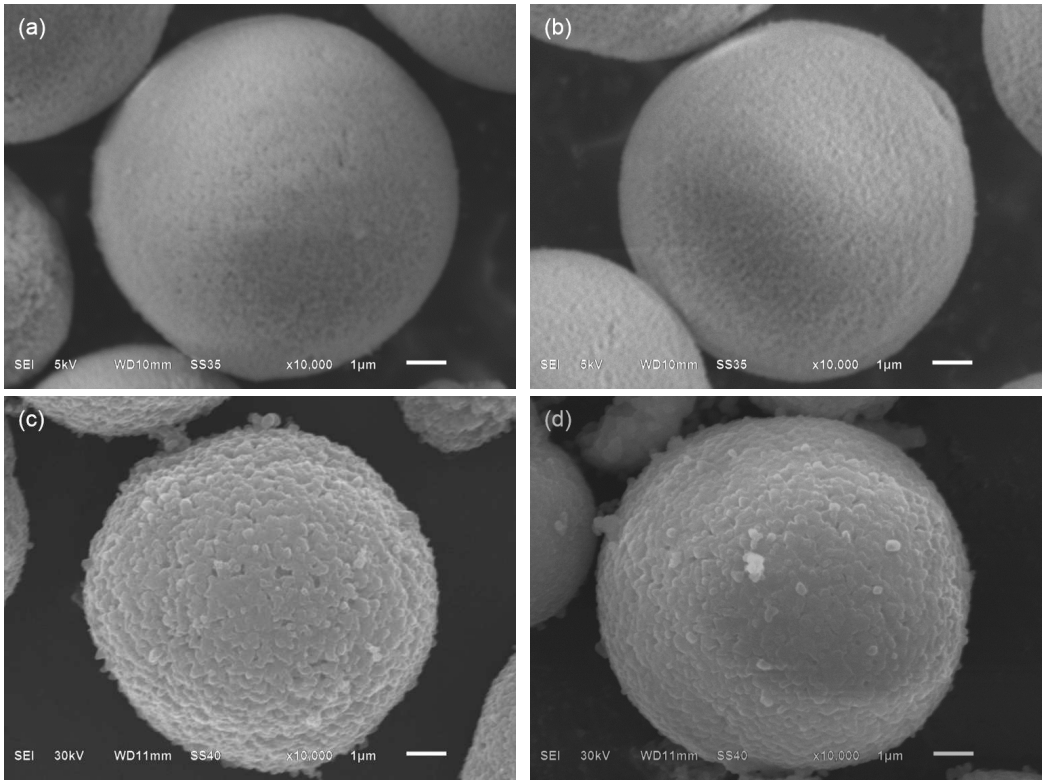

Fig. 1 SEM images of (a) MP precursor, (b) CP precursor, (c) MSL cathode material and (d) CL cathode material.

In order to directly observe the internal structure of the MP precursor and its corresponding MSL cathode material, these spherical particles were cut by a focused ion beam, and then SEM measurement on the cross-section of the particles was carried out. To further determine the composition changes in the MP precursor and MSL cathode material, EDXS data on the cross-section of the particles were collected. It can be found from the SEM images of the cross-section of precursor particles that the internal structure of the precursor is quite compact and intact (Fig. 2a and c). Fig. 2c displays the EDXS tests on four points from the core to the surface of the single precursor particle. The concentrations of Mn, Co, and Ni were plotted as a function of distance from the center to the surface of the precursor particle, as shown in Fig. 2e.

The Mn concentration remains almost constant across the particle (~75.0%). The relative Ni composition decreases from 24.6% in the center of the particle to 5.3% near the outer surface while the Co composition is nearly zero at the particle center and increases gradually to 19.9% near the outer surface. These results are consistent with the designed values. As shown in Fig. 2b and d, it's clear that the microsphere of MSL cathode material has an inner core and hierarchically multilayer concentric circle shells with porous structure. Also, the void space between the multilayer shells can be clearly seen. The EDXS results performed on the cross-section of the single microsphere confirm further that the inner core of the microsphere is consisted of a molar ratio of 0.750 Mn, 0.216 Ni and 0.034 Co. In addition, in the hierarchically multilayer shells, the molar ratio of Ni gradually decreases from 0.174 to 0.092 and the molar ratio of Co increases from 0.079 to 0.156, while the molar ratio of Mn remains almost constant (Fig. 2d and f). The distribution of Ni, Co and Mn in the MSL cathode material is a little different from that of the precursor, and it might be caused by the inter-diffusion of transition metals during the calcination process. Based on above analyses, it can be confirmed that the spherical $Li_{1.5}[Mn_{0.75}Ni_{0.15}Co_{0.10}]O_{2+\delta}$ cathode material with multilayer shells is successfully synthesized as desired.

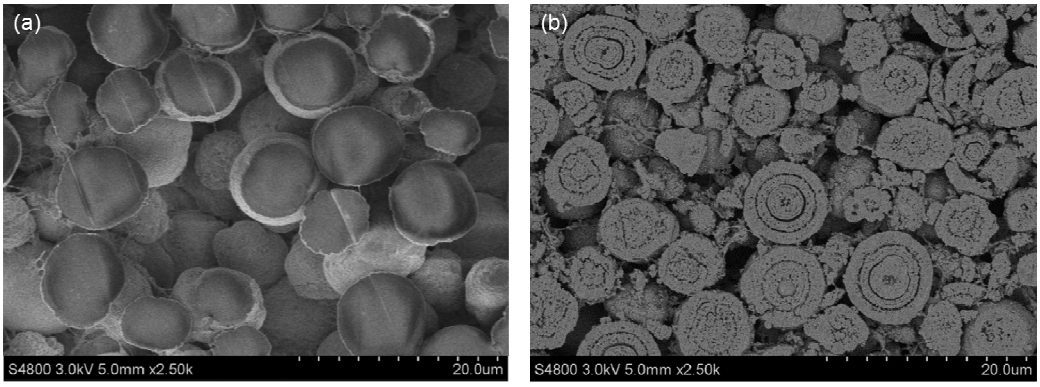

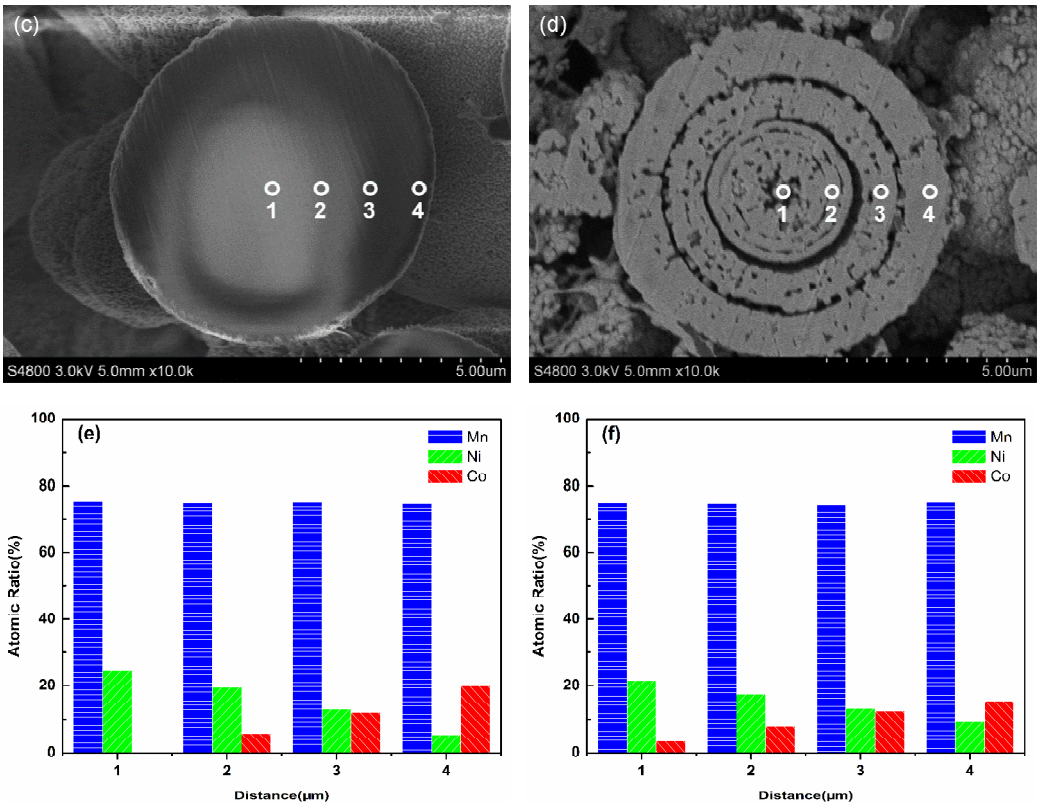

Fig. 2 SEM images of the cross-section of (a, c) MP precursor and (b, d) corresponding MSL cathode material; (e) and (f) EDXS compositional change from the center to the surface on the labeled points 1 to 4 of the cross-section of the MP precursor in the Fig. (c) and MSL cathode material in the Fig. (d).

Fig. 3a shows the XRD patterns for the MP and CP precursors. All the diffraction peaks of the precursors can be indexed as a typical hexagonal structure with a space group of R-3c,[24] which corresponds to standard $MnCO_3$ (JCPDS NO. 44-1472).[26] The diffraction peaks are broadened, it is probably because the particles consist of a lot of nano-scale primary grains.[27] After reacted with Li_2CO_3 at high temperature, the diffraction peaks become much narrower (Fig. 3b), indicating the MSL and CL cathode materials have high crystallinity. In addition, the diffraction peaks can be indexed based on a hexagonal α-$NaFeO_2$ type structure with the $R\bar{3}m$ space group,[28]

except for some weak peaks between 20° and 25°. These peaks between 20° and 25° can be observed in Li_2MnO_3-based oxides (space group C/2m) and might be caused by the superlattice ordering of the Li, Ni, Co and Mn in the 3a site.[5, 29] The lattice parameters of the MSL cathode material were determined to be 0.2850 nm for a and 1.4235 nm for c, using only the $R\bar{3}m$ space group during Rietveld refinements, which are close to that of CL cathode material (0.2852 nm for a, 1.4238 nm for c). The sharp diffraction peaks and the well resolved splits of (006)/(102) facets and (018)/(110) facets reflections for the MSL and CL cathode materials indicate the formation of a well-ordered layer structure.[30, 31] Besides, there were no representative peaks to indicate any impurity phase detected in these patterns.

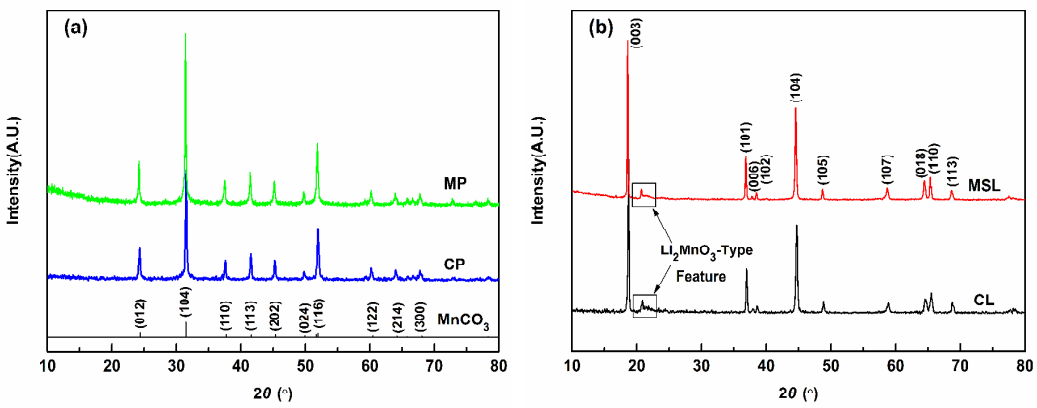

Fig. 3 XRD diffraction patterns of (a) MP and CP precursors and (b) MSL and CL cathode materials.

The electrochemical properties of the MSL cathode material were investigated using 2025 coin-type cells. The CL cathode material was also studied as a comparison. Fig. 4a and b show the initial and second charge/discharge curves of the Li/MSL cell and Li/CL cell at a rate of 0.1 C (1 C refers to 200 mA g^{-1} current density) in the

voltage range of 2.0-4.6 V, correspondingly. It's obvious that both the cathode materials display the representative profiles of the lithium-rich layered materials. In addition, the curves of these two cathode materials exhibit two distinguished regions, a sloping region below 4.5 V and a long plateau region around 4.5 V, during the initial charge process. The sloping region corresponds to the oxidation of the transition metal ions and the Li^+ extraction from the $LiMO_2$ component (M = Mn, Co, Ni), while the following long plateau region around 4.5 V corresponds to the extraction of Li^+ from the Li_2MnO_3 component accompanied by an irreversible loss of oxygen from the lattice.[32] The ideal charge/discharge process in the first cycle can be expressed by the following reactions (1), (2) and (3):[33]

$$x\mathrm{Li_2MnO_3}\cdot(1-x)\mathrm{LiMO_2} \rightarrow x\mathrm{Li_2MnO_3}\cdot(1-x)\mathrm{MO_2}+(1-x)\mathrm{Li} \quad (1)$$

$$x\mathrm{Li_2MnO_3}\cdot(1-x)\mathrm{MO_2} \rightarrow x\mathrm{MnO_2}\cdot(1-x)\mathrm{MO_2}+x\mathrm{Li_2O} \quad (2)$$

$$x\mathrm{MnO_2}\cdot(1-x)\mathrm{MO_2}+\mathrm{Li} \rightarrow x\mathrm{LiMnO_2}\cdot(1-x)\mathrm{LiMO_2} \quad (3)$$

Then, the plateau region around 4.5 V disappears in the second charge process, indicating an irreversible structure change during the first charge. Similar charge-discharge behavior in the first two cycles for lithium rich cathode has also been reported.[32, 34] As seen in Fig. 4a and b, the Li/MSL cell delivers a high discharge capacity of 257.8 mAh g^{-1} with initial coulombic efficiency of 77.8%, while the Li/CL cell delivers a slightly lower discharge capacity of 254.6 mAh g^{-1} with initial coulombic efficiency of 77.1%. Thus, the existence of the hierarchically multilayer shells doesn't cause a fading of capacity and decrease of coulombic efficiency.

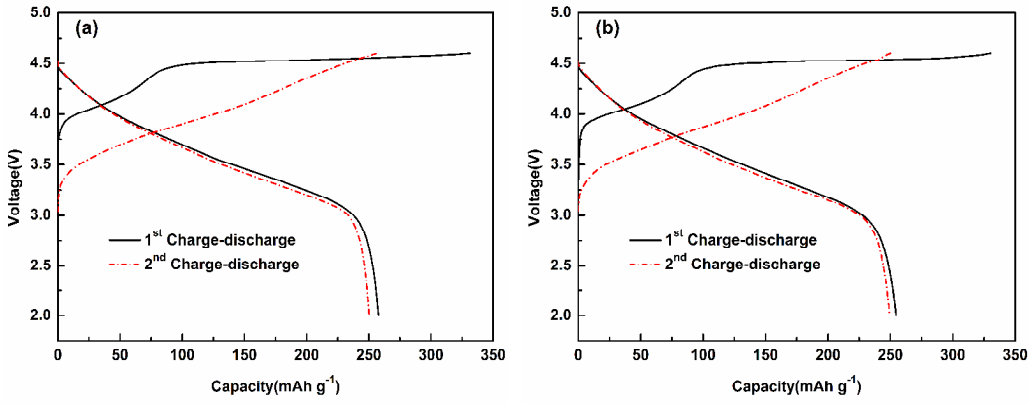

Fig. 4 Initial and second charge/discharge curves of (a) Li/MSL cell and (b) Li/CL cell at a rate of 0.1 C in the voltage range of 2.0-4.6 V.

In order to investigate the capacity retention of the as-prepared cathode materials, the cells were first charged/discharged at a rate of 0.1 C for activation, and then cycled at 0.5 C between 2.0 V and 4.6 V. Fig. 5 displays the cycle performance of the Li/MSL and Li/CL cells. The continuous charge/discharge curves of Li/MSL and Li/CL cells are shown in Fig. 5b and c, respectively. As being seen in Fig. 5a and b, the Li/MSL cell exhibits an initial discharge capacity of 224.6 mAh g^{-1} at 0.5 C and excellent cyclic stability, maintaining 96.1% of its initial capacity after 100 cycles. By contrast, the Li/CL cell shows a lower initial discharge capacity of 213.2 mAh g^{-1} and a rapid capacity fading with a capacity retention of only 88.7% over the same cycling period (Fig. 5c). The enhanced cycle performance of the MSL cathode material might benefit from the hierarchically multilayer shells structure. Such type of structure is supposed to effectively buffer and suppress large volume swing during Li^+ insertion/extraction process, so as to keep stable in the charge/discharge process.[20-22, 35] In addition, some researchers found that the lower concentration of Ni in the outer

layer of material can reduce side reactions between highly reactive Ni^{4+} and the electrolyte when charging to high voltage, which can keep the electrode/electrolyte interface to stable during the Li^{+} insertion/extraction process.[16, 36-38] In the hierarchically multilayer shells, Ni content is gradually decreased from the inner to outer surface of the particle. The content of the unstable Ni^{4+} in the outer layer of MSL cathode material can be reduced. In addition, the cycle performance of conventional spherical $Li_{1.5}Mn_{0.75}Ni_{0.25}O_{2+\delta}$ (denoted by CNL) cathode material was also investigated as a comparison. As shown in Fig. S1, the Li/CNL cell exhibits an initial discharge capacity of 205.2 mAh g^{-1} at 0.5 C between 2.0 V and 4.6 V. After 100 cycles, its capacity retention is about 86.9%. As a result, the multilayer spherical $Li_{1.5}[Mn_{0.75}Ni_{0.15}Co_{0.10}]O_{2+\delta}$ cathode material can exhibit more outstanding cycle performance than the conventional cathode material due to the hierarchically multilayer shells structure. Furthermore, the morphologies of the cycled MSL, CL and CNL electrodes after 100 cycles at 0.5 C are shown in Fig. 6 and Fig. S2. It can be found that the MSL particles still retain intact sphere morphologies after the long-term cycles (Fig. 6a and c), while some CL (Fig. 6b and d) and CNL (Fig. S2) particles crack and pulverize. These results can further confirm that the hierarchically multilayer shells structure can enhance the structural stability of the material during charge/discharge process.

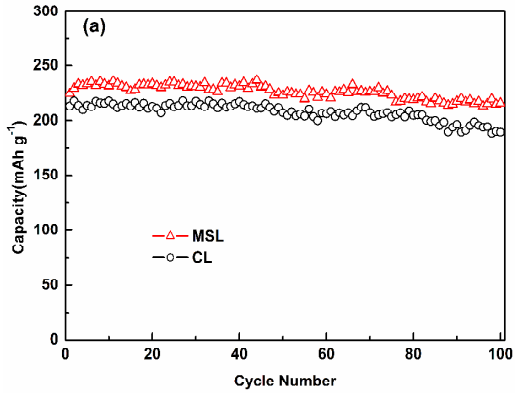

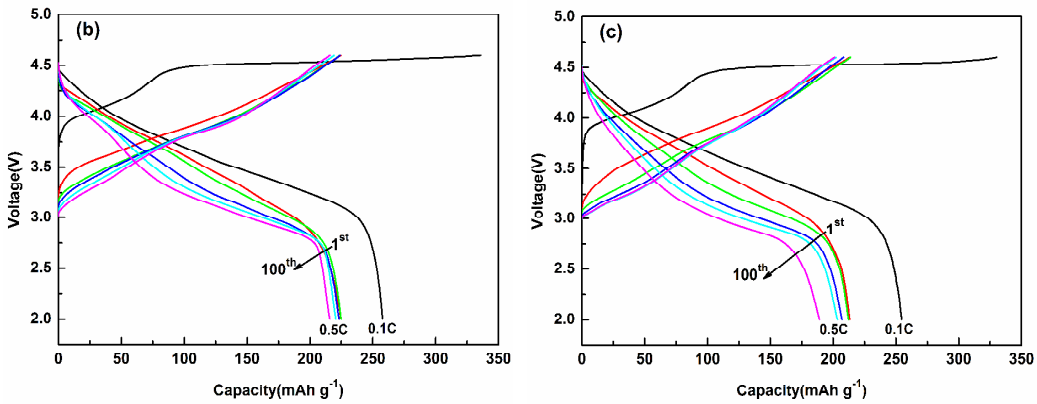

Fig. 5 (a) Capacity retention of Li/MSL cell and Li/CL cell; the continuous charge/discharge curves of the 1st, 50th, 75th, 100th cycles for (b) Li/MSL cell and (c) Li/CL cell at a rate of 0.5 C in the voltage range of 2.0-4.6 V.

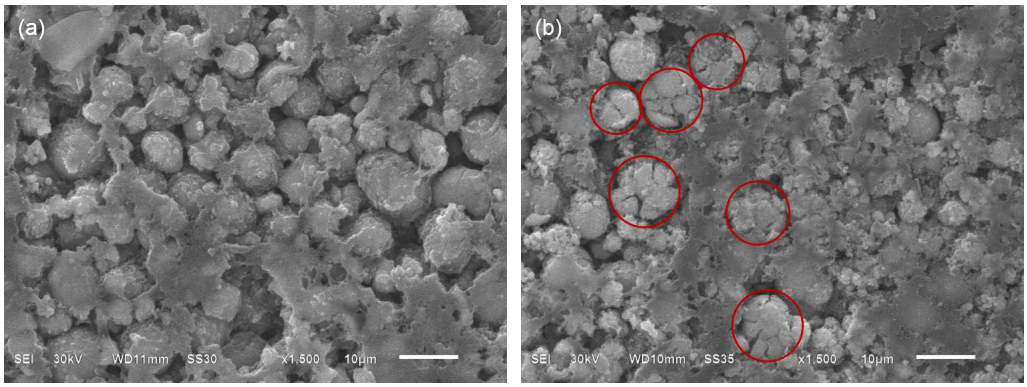

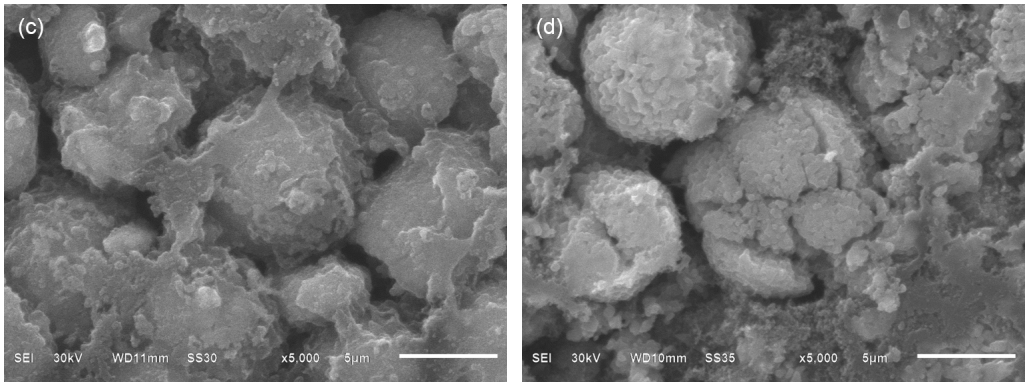

Fig. 6 SEM images of (a, c) MSL and (b, d) CL electrodes after 100 cycles.

To evaluate the rate capability of the as-prepared cathode materials, the testing cells were first charged and discharged five times at 0.1 C rate, then charged at 0.2 C and discharged at 0.2 C, 0.5 C, 1 C, 2 C 5 C and 10 C rates for 5 cycles in the voltage range of 2.0-4.6 V. After cycling at 10 C rate, the cells were cycled at 0.1 C again. The results are shown in Fig. 7a. Besides, Fig. 7b and c correspond to the discharge curves of Li/MSL cell and Li/CL cell at different discharge rates, respectively. Both Li/MSL cell and Li/CL cell present the dropped capacities along with the increased discharge current densities. However, no matter which discharge rate is adopted, the discharge capacity of MSL cathode material is always higher than the CL cathode material. Especially at a high discharge rate of 10 C, the Li/MSL cell shows a high discharge capacity of 102.7 mAh g^{-1}, whereas only 64.9 mAh g^{-1} specific capacity can be obtained for the Li/CL cell at the same rate. Furthermore, the capacity of the MSL cathode material is quickly recovered after returning to the 0.1 C rate during the rate capability test, which indicates the excellent cycle stability of the MSL cathode material. Furthermore, the Li/MSL cell displays an improved rate capability compared with the Li/CNL cell, as illustrated as Fig. S3. Accordingly, the improvement of the

cycle performance and rate capability of the MSL cathode material mainly benefit from the special architecture.

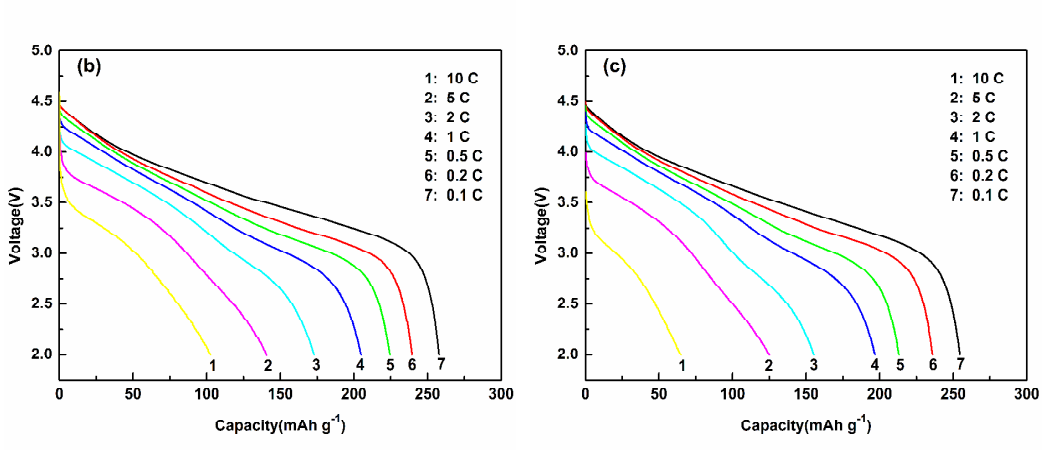

Fig. 7 (a) Discharge capacity versus cycle number of Li/MSL cell and Li/CL cell; discharge curves of (b) Li/MSL cell and (c) Li/CL cell at various rates in the voltage range of 2.0-4.6 V.

As well known, the rate capability of the cathode materials is relevant to the electrochemical insertion/extraction of Li^+.[20-22] To further discuss diffusion velocity of Li^+ in the as-prepared cathode materials, the GITT test as a reliable technique to quantize the chemical diffusion coefficient of Li^+ in electrode materials was carried out. Fig. 8a and b show the GITT curves of Li/MSL and Li/CL cells during the second cycles as a function of time in the voltage range of 2.0-4.6 V, respectively. The

differential factor dE/dx can be determined by the relationship between Es and stoichiometry x during the delithiation process, then the dE/dx as a function of stoichiometry x can be acquired, and the function image is shown in Fig. 8c. Similarly, the dE/d$t^{1/2}$ as a function of stoichiometry x can also be obtained during the delithiation process, and the result is shown in Fig. 8d. The values of dE/dx and dE/d$t^{1/2}$ are the key parameters calculating the chemical diffusion coefficient of Li^+ (D_{Li^+}). The D_{Li^+} values can be determined by Fick's second law of diffusion and calculated according to the following equation (1):

$$D_{Li^+} = \frac{4}{\pi}\left(I_0 \frac{V_m}{FS}\right)^2 \left(\frac{dE/dx}{dE/dt^{1/2}}\right)^2, \quad t << \frac{L^2}{D_{Li^+}} \tag{1}$$

where I_0 (A) is the applied current in the charge/discharge process, V_m (cm^3 mol^{-1}) is the molar volume of compound, which is deduced from the crystallographic data, F (C mol^{-1}) is the Faraday constant, S (cm^2) is the surface area of the electrode, and L (cm) is the diffusion length.

The D_{Li^+} values are calculated by the equation (1), as shown in Fig. 8e. It can be found that the D_{Li^+} values of MSL cathode material are in the range from 7.54×10^{-12} to 1.36×10^{-10} cm^2 s^{-1}, while the D_{Li^+} values of CL cathode material are in the range from 5.20×10^{-12} to 8.72×10^{-11} cm^2 s^{-1}, during the delithiation process. It must be mentioned that the D_{Li^+} values of MSL and CL cathode materials are almost constant, when the stoichiometry x is in the range from 0.5 to 0.9, and the D_{Li^+} values of MSL cathode material are apparently higher than those of CL cathode material. In addition, the D_{Li^+} values of CNL cathode material are in the range from 8.71×10^{-13} to 8.06×10^{-11} cm^2 s^{-1} (Fig. S4). And the D_{Li^+} values are also far lower

than those of the MSL cathode material.

All of the improved electrochemical properties of the spherical cathode material with multilayer shells are ascribed to the special architecture. The presence of the void space between the hierarchically multilayer shells could serve as a reservoir for electrolyte and allow much easier penetration of the electrolyte into the inside of the microspheres, hence resulting in facilitating the electrochemical insertion/extraction of Li^+. In addition, the particular structure can effectively buffer and suppress large volume swing during Li^+ insertion/extraction process, so as to keep stable morphology in the charge/discharge process. Therefore, the design of the microspheres with hierarchically multilayer shells structure will be a new and effective approach to achieve high-performance electrode materials.

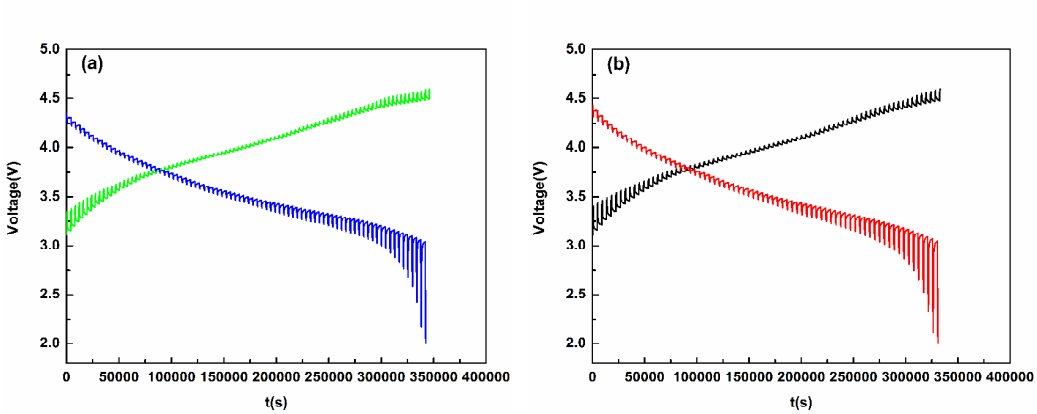

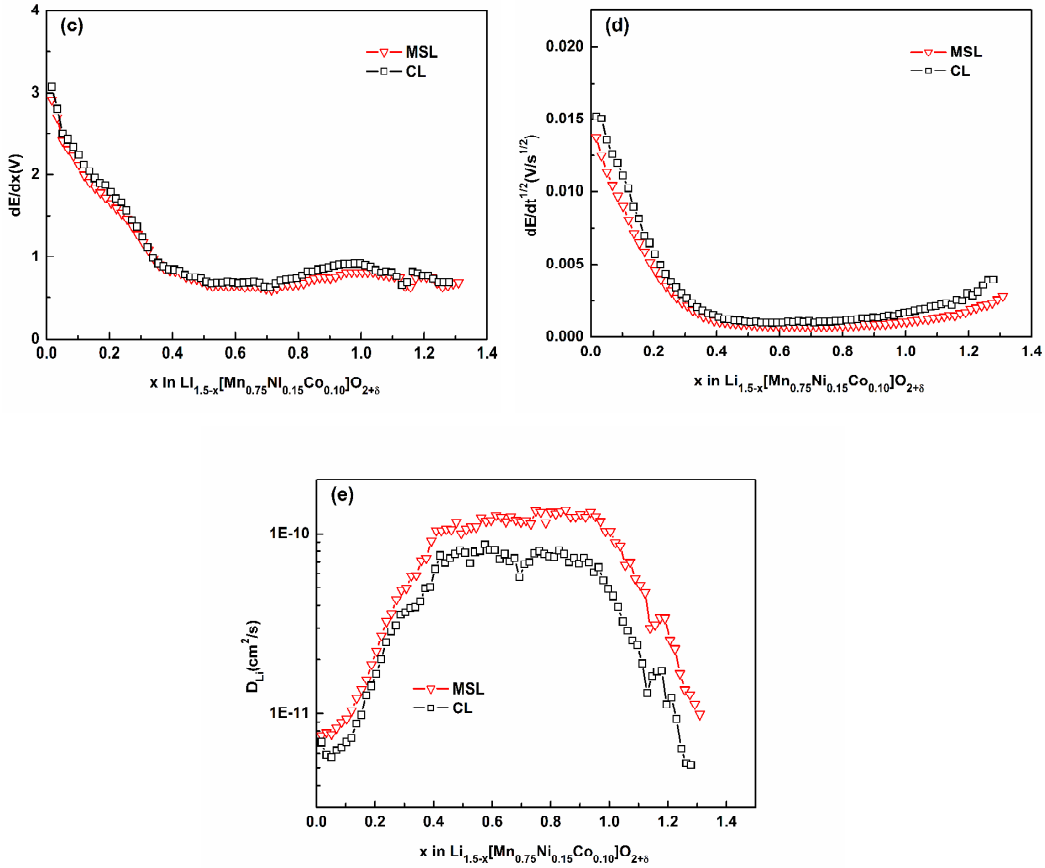

Fig. 8 The GITT curves of (a) MSL and (b) CL cathode materials as a function of time in the voltage range of 2.0-4.6 V; (c) dE/dx and (d) dE/d$t^{1/2}$ as a function of the stoichiometry x; and (e) the calculated D_{Li^+} values of the MSL and CL cathode materials as a function of the stoichiometry x.

4. Conclusions

The spherical $Li_{1.5}[Mn_{0.75}Ni_{0.15}Co_{0.10}]O_{2+\delta}$ cathode material with hierarchically multilayer shells structure was successfully synthesized through layer-by-layer self-assembly with a co-precipitation process for the first time. The microsphere is composed of an inner core and a hierarchically multilayer concentric circle shells with

porous structure. The void space between layers can probably show the buffering action for volume change during charge/discharge process and serve as a reservoir for electrolyte which allows much easier penetration of the electrolyte into the inside of the microspheres. Accordingly, the spherical cathode material with multilayer shells exhibits excellent electrochemical performances. It reveals a relatively high discharge capacity of 257.8 mAh g^{-1} at a rate of 0.1 C and outstanding cyclability with a capacity retention of 96.1% after 100 cycles at a rate of 0.5 C in the voltage range of 2.0-4.6 V, while the conventional material $Li_{1.5}[Mn_{0.75}Ni_{0.15}Co_{0.10}]O_{2+\delta}$ and $Li_{1.5}[Mn_{0.75}Ni_{0.25}]O_{2+\delta}$ display only 88.7% and 86.9%, respectively. Most importantly, the rate capability of the spherical cathode material with multilayer shells was significantly better than the conventional cathode material. Even at a high discharge rate of 10 C, the multilayer spherical cathode material can deliver a high discharge capacity of 102.7 mAh g^{-1} between 2.0 and 4.6 V. Thus, the spherical $Li_{1.5}[Mn_{0.75}Ni_{0.15}Co_{0.10}]O_{2+\delta}$ cathode material with multilayer shells is a promising positive material with high performance for the application of lithium-ion batteries.

Acknowledgements

This work was funded by the National Natural Science Foundation of China under project No. 51272221, Scientific and Technical Achievement Transformation Fund of Hunan Province under project No. 2012CK1006, Key Project of Strategic New Industry of Hunan Province under project No. 2013GK4018, and Science and Technology Plan Foundation of Hunan Province under project no. 2013FJ4062.

Notes and references

1 B. C. Melot and J. M. Tarascon, *Acc. Chem. Res.*, 2013, **46**, 1226.

2 M. Armand and J. M. Tarascon, *Nature*, 2008, **451**, 652.

3 A. Manthiram, *J. Phys. Chem. Lett.*, 2011, **2**, 176.

4 B. Scrosati and J. Garche, *J. Power Sources*, 2010, **195**, 2419.

5 M. M. Thackeray, S. H. Kang, C. S. Johnson, J. T. Vaughey, R. Benedek and S. A. Hackney, *J. Mater. Chem.*, 2007, **17**, 3112.

6 C. R. Fell, D. H. Lee, Y. S. Meng, J. M. Gallardo-Amores, E. Morán and M. E. A. Dompablo, *Energy Environ. Sci.*, 2012, **5**, 6214.

7 H. Deng, I. Belharouak, R. E. Cook, H. Wu, Y. K. Sun and K. Amine, *J. Electrochem. Soc.*, 2010, **157**, A447.

8 Y. Gao, J. Ma, X. Wang, X. Lu, Y. Bai, Z. Wang and L. Chen, *J. Mater. Chem. A*, 2014, **2**, 4811.

9 Z. Lu and J. R. Dahn, *J. Electrochem. Soc.*, 2002, **149**, A815.

10 P. Lanz, H. Sommer, M. Schulz-Dobrick and P. Novák, *Electrochimica. Acta*, 2013, **93**, 114.

11 N. Yabuuchi, K. Yoshii, S. T. Myung, L Nakai and S. Komaba, *J. Am. Chem. Soc.*, 2011, **133**, 4404.

12 T. A. Arunkumar, Y. Wu and A. Manthiram, *Chem. Mater.*, 2007, **19**, 3067.

13 H. Xu, S. Deng and G. Chen, *J. Mater. Chem. A*, 2014, **2**, 15015.

14 G. Singh, R. Thomas, A. Kumar and R. S. Katiyar, *J. Electrochem. Soc.*, 2012, **159**, A410.

15 D. Wang, Y. Huang, Z. Huo and L. Chen, *Electrochimica. Acta*, 2013, **107**, 461.

16 Y. K. Sun, D. H. Kim, C. S. Yoon, S. T. Myung, J. Prakash and K. Amine, *Adv. Funct. Mater.*, 2010, **20**, 485.

17 Z. X. Chi, W. Zhang, X. S. Wang, F. Q. Cheng, J. T. Chen, A. M. Cao and L. J. Wan, *J. Mater. Chem. A*, 2014, **2**, 17359.

18 M. M. Ren, Z. Zhou, X. P. Gao, W. X. Peng and J. P. Wei, *J. Phys. Chem. C*, 2008, **112**, 5689.

19 Q. Wang, D. A. Zhang, Q. Wang, J. Sun, L. L. Xing and X. Y. Xue, *Electrochimica. Acta*, 2014, **146**, 411.

20 X. W. Lou, L. A. Archer and Z. Yang, *Adv. Mater.*, 2008, **20**, 3987.

21 J. Liu, H. Xia, D. Xue and L. Lu, *J. Am. Chem. Soc.*, 2009, **131**, 12086.

22 X. Wang, X. L. Wu, Y. G. Guo, Y. Zhong, X. Cao, Y. Ma and J. Yao, *Adv. Funct. Mater.*, 2010, **20**, 1680.

23 S. Yang, X. Wang, Q. Chen, X. Yang, J. Li and Q. Wei, *J. Solid State Electrochem.*, 2012, **16**, 481.

24 S. H. Park, S. H. Kang, I. Belharouak, Y. K. Sun and K. Amine, *J. Power Sources*, 2008, **177**, 177.

25 H. Deng, I. Belharouak, Y. K. Sun and K. Amine, *J. Mater. Chem.*, 2009, **19**, 4510.

26 S. Zhang, C. Deng, B. L. Fu, S. Y. Yang and L. Ma, *Powder Technol.*, 2010, **198**, 373.

27 D. K. Lee, S. H. Park, K. Amine, H. J. Bang, J. Parakash and Y. K. Sun, *J. Power Sources*, 2006, **162**, 1346.

28 S. J. Shi, J. P. Tu, Y. Y. Tang, Y. X. Yu, Y. Q. Zhang and X. L. Wang, C. D. Gu, *J. Power Sources*, 2013, **228**, 14.

29 M. M. Thackeray, C. S. Johnson, J. T. Vaughey, N. Li and S. A. Hackney, *J. Mater. Chem.*,

2005, **15**, 2257.

30 J. M. Zheng, X. B. Wu and Y. Yang, *Electrochimica. Acta*, 2011, **56**, 3071.

31 G. Singh, R. Thomas, A. Kumar, R. S. Katiyar and A. Manivannan, *J. Electrochem. Soc.*, 2012, **159**, A470.

32 A. R. Armstrong, M. Holzapfel, P. Novák, C. S. Johnson, S. H. Kang, M. M. Thackeray and P. G. Bruce, *J. Am. Chem. Soc.*, 2006, **128**, 8694.

33 C. S. Johnson, N. Li, C. Lefief and M. M. Thackeray, *Electrochem. Commun*, 2007, **9**, 787.

34 C. S. Johnson, N. Li, C. Lefief , J. T. Vaughey and M. M. Thackeray, *Chem. Mater.*, 2008, **20**, 6095.

35 L. Su, Y. Jing and Z. Zhou, *Nanoscale*, 2011, **3**, 3967.

36 Y. K. Sun, D. H. Kim, H. G. Jung, S. T. Myung and K. Amine, *Electrochimica. Acta*, 2010, **55**, 8621.

37 S. U. Woo, C. S. Yoon, K. Amine, I. Belharouak and Y. K. Sun, *J. Electrochem. Soc.*, 2007, **154**, A1005.

38 D. P. Abraham, R. D. Twesten, M. Balasubramanian, J. Kropf, D. Fischer, J. McBreen, I. Petrov and K. Amine, *J. Electrochem. Soc.*, 2003, **150**, A1450.

The Table of Contents entry

Graphic:

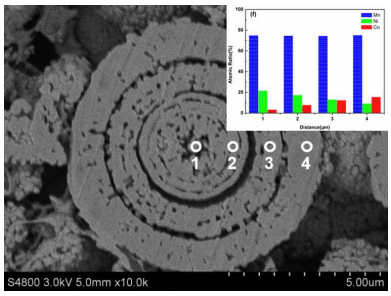

Text:

$Li_{1.5}Mn_{0.75}Ni_{0.15}Co_{0.10}O_{2+\delta}$ microspheres with hierarchically multilayer concentric circle shells as the cathode materials for lithium-ion batteries.